Pore-scale precipitation pattern and grain-scale cementation strength by microbially induced calcium carbonate precipitation (MICP)

Tae-Hyuk Kwon[1#], *Soo-Min* Ham[2], *Seung-Hun* Baek[1], *Gyeol* Han[1], *Alejandro* Martinez[2], and *Jason* DeJong[2]

[1]*Korea advanced institute of Science and Technology, Department of Civil and Environmental Engineering, 291 Daehakro 291, Dajeon, South Korea*
[2]*University of California, Davis, Civil and Environmental Engineering, One Shields Avenue, Davis, CA, USA*
[#]*Corresponding author: t.kwon@kaist.ac.kr*

ABSTRACT

Microbial induced calcium carbonate precipitation (MICP) is widely investigated as a sustainable method of soil improvement. The pore-scale precipitation habit of calcium carbonate ($CaCO_3$) and the grain-scale mechanical strength of the cementing bonds play a significant role in determining the mechanical response of MICP-treated soils. This study presents the pore-scale precipitation patterns in MICP-treated sands and the grain-scale cementation strength of two beads cemented by MICP. X-ray computed microtomography imaging of MICP-treated sands with different grain sizes reveal that the surface area, number of contacts, and flow-induced shear detachment as well as bacterial cell loci have a profound effect on the pore-scale precipitation. With different grain size, the precipitation can show either a contact-cementing pattern or a surface-coating habit. Particularly, evolution of the precipitation pattern is observed for large-sized grains from the surface-coating mode to the contact-cementing mode with an increase in $CaCO_3$ content. The grain-scale mechanical strength tests on MICP-bonded bead pairs demonstrate that the failure with MICP bonding occurs in three modes: debonding, internal, and mixed failure modes. Amongst, the debonding failure mode has the greatest strength and the internal failure mode shows the lowest strength. The tensile strength is greater than the shear strength in all modes; particularly in debonding failure mode, the tensile strength of ~35 kPa and shear strength of ~13 kPa. The presented results advance our insight into pore-scale and grain-scale behavior of MICP-treated sands, which can be further extended to develop DEM models and transport models.

Keywords: MICP; precipitation pattern; tensile strength; shear strength; mechanical failure mode

1. Introduction

Microbially induced calcium carbonate precipitation (MICP) is widely investigated as a potential way of soil improvement techniques (Mitchell and Ferris, 2005; Whiffin et al., 20017; DeJong et al., 2010; Lin et al., 2016). The MICP produces calcium carbonate minerals that bonds grains and increase soil strength (Lin et al., 2016; Seifan and Berenjian, 2019). Previous studies have demonstrated through laboratory tests (DeJong et al., 2006; van Paassen, 2011; Cheng et al., 2013; Al Qabany and Soga, 2013; Nafisi et al., 2019) and field demonstrations that the MICP treatment increases the soil strength and stiffness (van Paassen, 2010; Gomez et al., 2015; Darby et al., 2019; Bick et al., 2019).

The location of calcium carbonate ($CaCO_3$) precipitation in pores and the resulting bonding strength heavily affect mechanical responses of MICP-treated soils. Numerous efforts have been undertaken to analyze the spatial distribution of $CaCO_3$ at a pore scale (or a grain scale) using X-ray computed microtomography (X-ray CMT), scanning electron microscopy (SEM), energy dispersive spectroscopy (EDS), and S-wave monitoring (Lin et al., 2016; Terzis and Laloui, 2018; Mahawish et al., 2019; Ham et al. 2022). However, pore-scale (or grain-scale) $CaCO_3$ precipitation patterns remain poorly understood because the resulting precipitation patterns are heavily influenced by the treatment conditions, including but not limited to soil type, grain size, cell density of inoculums, ureolysis rate, solution concentration. Meanwhile, recently published studies by Ham et al. (2022) and Lin et al. (2022) have examined the grain-scale cementation strength by using two beads pairs. Those studies are limited to spherical glass beads greater than 1 mm in diameter. This brings a question whether the observations would be valid in natural sands with smaller diameters and various grain size distributions.

This paper presents the pore-scale precipitation patterns in sands using X-ray CMT imaging, and the test results on the grain-scale tensile and shear strengths of two beads cemented by MICP. The MICP patterns are compared with the idealized precipitation models, and the effects of grain size and solution concentration are discussed. Then, the mechanical failure modes are related to the $CaCO_3$ content and the grain-scale shear and tensile strengths of cemented beads.

2. Material and Methods

2.1. Model bacteria

Model bacteria *Sporosarcina pasteurii* (American Type Culture Collection, ATCC 11859) was used due to their high ureolysis activity (Zhao et al., 2014). An ammonium-yeast extract medium was used as a liquid growth medium to culture the bacterial inoculum; it contained 20 g/L yeast extract, 10 g/L ammonium sulfate ($(NH_4)_2SO_4$), and 0.13 M Tris buffer (pH = 9.0), following the suggestion by ATCC 1376. The bacteria *S. pasteurii* were cultured aerobically in the growth media at 30°C in a shaking incubator at 200 rpm for ~20 hours, at which the optical density (OD_{600}) were mostly greater than 1.0. The bacterium culture was then centrifuged at 4000 g for 40 min, after which the supernatant was taken out and new growth media was added. This was used as a bacterial inoculum for MICP treatments, and this inoculum was stored at 4°C prior to use.

2.2. MICP treatment for X-ray CMT Imaging

Four poorly-graded sands (Cape May Formation, NJ, USA) were used in this study, which were named as 100A, 100B, 100C, and 100D. These sands 100A, 100B, 100C, and 100D have the mean grain size (D_{50}) of 0.21, 0.50, 1.30, and 2.95 mm, respectively (Sturm, 2019; Pires-Stum and DeJong, 2022). First, a dry sand pack was prepared a rigid-walled cylindrical polycarbonate column for X-ray CMT imaging. The prepared column was vertically stressed with ~100–150 kPa using springs at the top to prevent any movement of particles. More details about column preparations can be found in Baek (2022) and Baek et al. (2023).

Upward-injecting MICP treatments consisted of three phases, and the first phase is the inoculation of the model bacteria. Three pore volumes of the bacterial solution (~330 mL) were injected at a constant flow rate, after which a retention time more than 36 h followed for the bacteria to attach on sand grains. The second phase is the injection of the rinsing solution for three pore volumes (25 mM of ammonium chloride, 42.5 mM of sodium acetate, and 154 mM of sodium chloride). This rinsing solution was injected at a constant flow rate, which promoted the bacterial attachment with sodium chloride while flushing out the suspended bacteria in pore spaces. Lastly, the third phase immediately began with the injection of the cementation solution for three pore volumes (300 mM of calcium chloride and urea, 25 mM of ammonium chloride, 42.5 mM of sodium acetate, and 0.2 g/L of yeast extract) at a constant flow rate. Thereafter, a retention time more than 20 h was given for completion of the MICP reaction under no-flow condition. The third phase, cementation solution injection, was repeated every day until a $CaCO_3$ content (CC) of ~15–25% was achieved.

2.3. X-ray CMT Imaging

Upon completion of the MICP treatment, each sand pack column was disassembled, and MICP-treated sand samples of ~1 cm^3 were collected for high-resolution X-ray CMT imaging. The X-ray CMT facility contains the nanofocus open X-ray source tube with the focal spot size of 400 nm and the flat panel detector with 2,048 × 2,048 pixels. Total 2,048 sliced images were obtained for each MICP-treated sand sample, in which a sliced image is composed of 2,048 × 2,048 pixels with a pixel size and depth of ~3–8 μm.

2.4. MICP treatment for two bead pair tests

The uniform-sized spherical glass beads with the diameter of 3 mm were used for grain-scale cementation strength tests. The dry beads were pluviated and packed in a rigid-walled polycarbonate column. This bead pack had the diameter of 60 mm and the height of 90 mm.

The MICP treatment method follows the aforementioned procedure with three phases for X-ray CMT imaging. These phases were the injections of bacterial inoculum, rinsing solution, and cementation solution. The compositions of rinsing solution and cementation solutions were slightly modified. The inoculum of bacteria *S. pasteurii* was injected into the column for three pore volumes. The injection rate was set to be 10 mL/min in all injections. The bacteria were then retained for 24 hours under no mass flux to facilitate attachment of bacteria onto the bead surfaces. Then, the column was flushed with the rinsing solution, composed of 9 g/L of sodium chloride (NaCl) solution, for two pore volume. High ionic concentration can enhance the attachment of bacteria and distribute bacteria homogeneously (Harkes et al., 2010). In addition, the flushing process can remove the suspended bacteria and sulfate ion which has an opportunity to form gypsum with calcium ion. The cementation solution (350 mM of calcium chloride, 350 mM of urea, 250 mM of ammonium chloride, 42.5 mM of sodium acetate, and 0.2 g/L of yeast extract) was introduced into the column for two pore volume, and the retention time of 24 h was allowed until the next cementation treatment. As the spherical beads have relatively small surface areas and low grain contact number, bio-augmentation was regularly required. The bioaugmentation was repeated after every two cycles of the cementation treatment. First, the specimen was flushed with the 250 mM of ammonium chloride solution to avoid the reaction between the left-over calcium ions in pores and sulfate in the inoculum. Then, the bacterial inoculum was injected. This MICP treatment continued until a $CaCO_3$ content (CC) of ~17% was achieved. More details of MICP treatment procedures for those bead packs can be found in Ham et al. (2022).

2.5. Tensile and Shear tests

The treated bead pack was dried at 50°C for five days. The bead pack was extracted from the polycarbonate column. Then, the weight was measured to calculate the bulk CC of the treated specimen. Thereafter, the bead pack was manually split with care. From the fragments, two bonded bead pairs were chosen for testing. To remove the potential biases from this selection process, total 60 pairs, 30 pairs for tensile and shear tests each, were selected evenly within the specimen. In addition, the X-ray computed tomography (X-ray CT) imaging

was conducted on the selected bead pairs. These CT images allowed us to estimate the minimum cross-sectional areas which was later used to convert the measured force to stress.

The test configuration was designed to induce a failure of a bonded bead pair by a tensile load or a shear load. One side of a bead pair was attached to a movable piston, which was connected to the micrometer. The horizontal pull-out force was applied by controlling the displacement with the micrometer. The other side of a bead pair was attached on a relatively rigid stainless steel cantilever beam instrumented with strain gauges to measure the pull-out force. Four strain gauges attached on the cantilever beam, and they were connected as a full-bridge Wheatstone Bridge circuit to measure the bending of the beam. While a tensile or shear load is applied, the applied force was measured by the deflection of a cantilever beam and the attached strain gauges on the beam. In tensile tests, a bead pair was mounted horizontally, and in shear tests, a bead pair was mounted vertically. The developed test configuration is described in Ham et al. (2022).

The CC of the MICP-treated bead pair was measured after the mechanical test by using the acid washing method (Choi et al., 2017). The minimum cross-sectional area was obtained for each bead pair from the X-ray CT images, and assumed as the probable failure plane for stress calculation.

3. Grain-scale Precipitation Patterns

3.1. Calcite precipitation patterns in sands

The high-resolution images enable examining the pore-scale $CaCO_3$ precipitation patterns in MICP-treated sands. Representative 3D constructed images of 100A-to-D are shown in Figure 1. Figure 2 provides clear illustrations of the precipitated calcite in sands with different grain sizes. Herein, the phases were segmented using the threshold method.

In small-sized sands (100A and 100B), precipitation of calcite crystals mostly occurs at grain contacts. As the CC level increases, the calcite crystals grow and bridge neighboring sand grains. Apparently, this is more distinctively observed in smaller pores rather than larger pores. On the other hand, this preferential precipitation leaves large pores open and a considerable portion of the grain surfaces free of any precipitates (Figures 1a and 1b, Figures 2a and 2b). Note that the precipitation loci are heavily controlled by the loci of attached bacteria. Therefore, the observed preferential precipitation at grain contacts implies that bacteria are more likely to attach at grain contacts and small pores than to open grain surfaces exposed to pore spaces.

This result is possibly attributable to the bacteria attachment and detachment under repeated solution injections. During the treatment solution injections, a fluid flow induces shear detachment of the bacteria. A drag force due to the fluid flow can be relatively weak to cause detachment in the vicinity of the grain contacts. And, the bacteria in small pores can be filtered or strained by small pore throats. Whereas, it is expected that the bacteria attached on the exposed grain surfaces in large pores are more prone to shear detachment. Consequently, this preferential survival of attached bacteria dominantly caused the contact-cementing precipitation behavior in fine sands.

By contrast, a surface-coating (or grain-coating) type of precipitation habit was observed in coarse sands (100C and 100D; Figures 1c and 1d, Figures 2c and 2d). The surface-coating pattern shows that $CaCO_3$ crystals are evenly precipitated on the grain surfaces, resulting in a uniform coating of grains by $CaCO_3$ crystals. The observed precipitation pattern implies that inoculated bacteria were fairly evenly attached on grain surfaces, and caused a surface-coating type of $CaCO_3$ precipitation. This is presumably due to small surface area and low contact numbers which required frequent bio-augmentations in the MICP treatment tests. As the grain contacts are fewer in coarser sands, the repeated cementation solution injections detached and displaced a considerable amount of bacteria in the sand packs, which in turn lowered the urea hydrolysis rate. In coarse sands bio-augmentation was frequently required to maintain a level of urea hydrolysis rate and activity. By contrast, in fine sands, bacterial inoculation was conducted only once in the beginning.

The results show that bacterial attachment location plays a critical role in determining precipitation pattern while repeated fluid flows causes shear detachment and flushing of bacteria.

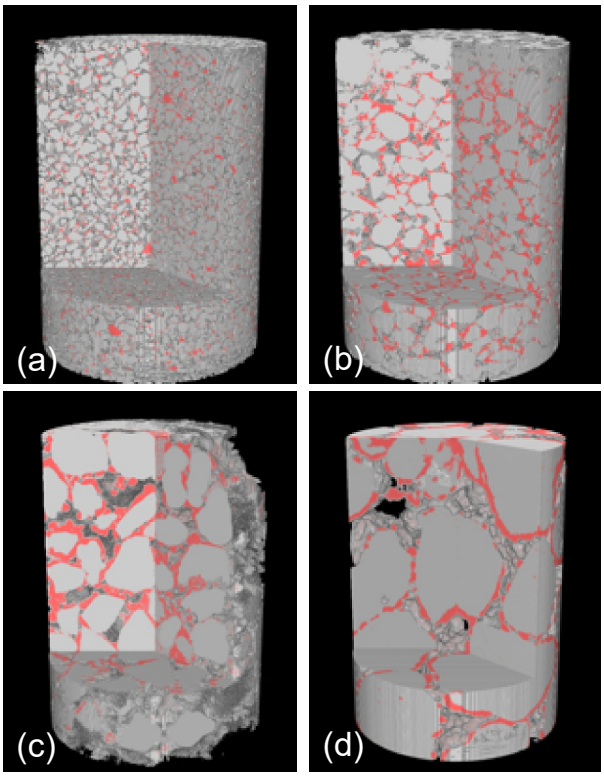

Figure 1. X-ray CMT 3D reconstructed images of MICP-treated sands: (a) 100A, (b) 100B, (c) 100C, and (d) 100D. (adopted from DeJong et al., 2022)

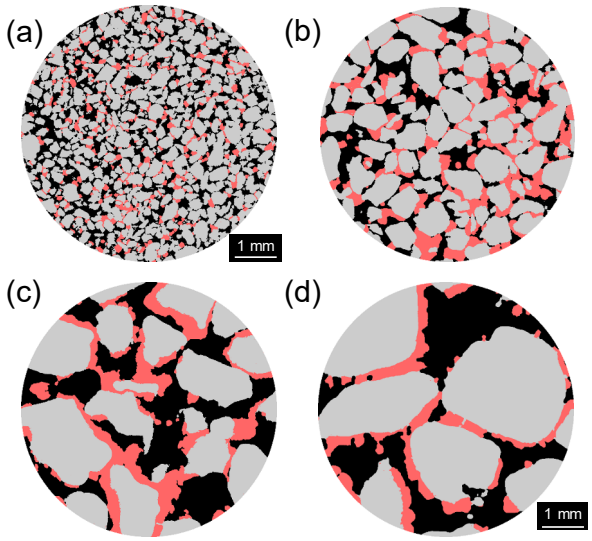

Figure 2. X-ray CMT XY-sliced images of MICP-treated sands: (a) 100A, (b) 100B, (c) 100C, and (d) 100D. (adopted from Baek, 2022). The CC values are estimated as CC = 14.2%, 18.2%, 21.3%, and 18.8%, respectively. Each phase is color-coded: gray = solid grains, pink = $CaCO_3$ minerals, and black = pore spaces (adopted from Baek et al., 2023).

3.2. Grain-scale precipitation models

From the above X-ray CMT images, three idealized models for the calcite precipitation patterns can be delineated: surface-coating, meniscus-filling, and flat torus-filling modes, as shown in Figure 4a. Geometric configurations of these models allow derivation of analytical formations to estimate the contact radius as a function of CC and grain diameter (Ham et al., 2022).

Figure 3 shows the estimated contact radii of the $CaCO_3$ bonded bead pairs with respect to their CC levels. The contact radius was computed from the minimum cross-sectional area estimated from the X-ray CT images. by assuming the equivalent circular area. The CC is the ratio of calcite contents to bead, and the large CC means that more calcite was precipitated as the uniform size of glass beads were used in this study. The results reveal that the contact radius linearly increases with the CC level. Furthermore, the data trend hardly follows one single model prediction, but it rather shows an evolution from the surface-coating mode to the flat-torus-filling mode as the CC level increases. The calcite precipitation shows a mixed surface-coating and meniscus-filling pattern at a low CC level (e.g., CC < 15%), and it evolves to a mixed meniscus-filling and flat torus-filling mode at a high CC level (e.g., CC > 20%), as also can be seen in Figure 4.

It is worth pointing out that this result was obtained from glass beads with 3-mm diameter. With such large-sized grains (sand and gravel), a surface-coating pattern was mostly observed due to the small specific surface area and ensuing frequent bio-augmentation. This is consistent with the results obtained from sands 100C and 100D, as shown in Figures 1 and 2.

As the CC level exceeds 20%, the cementation locally occurs at the grain contacts (menisci), and consequently, the meniscus-filling and flat torus-filling patterns become noticeable. Such a change from surface-coating to flat torus-filling with increasing CC is possibly due to the geometrical configuration by surrounding grains and the nutrient and cell transports through pores. In the beginning, the cementation continues to coat the bead surfaces where the bacteria exist. After a certain level of CC, there is not enough space to grow the $CaCO_3$ coating layer in uniform thickness, and thus homogeneous and even coating is no further possible because the coating becomes quite thick and bridges the neighbouring host grains. But, at grain contacts there is still space available for precipitation, in which the cells and nutrients are transported well. Nevertheless, it is worth pointing out that the observed cementation pattern and its evolution is limited to coarse-grained soils with the grain diameter greater than 1 mm. As previously mentioned, a surface-coating pattern was not observed in fine sands (100A and 100B).

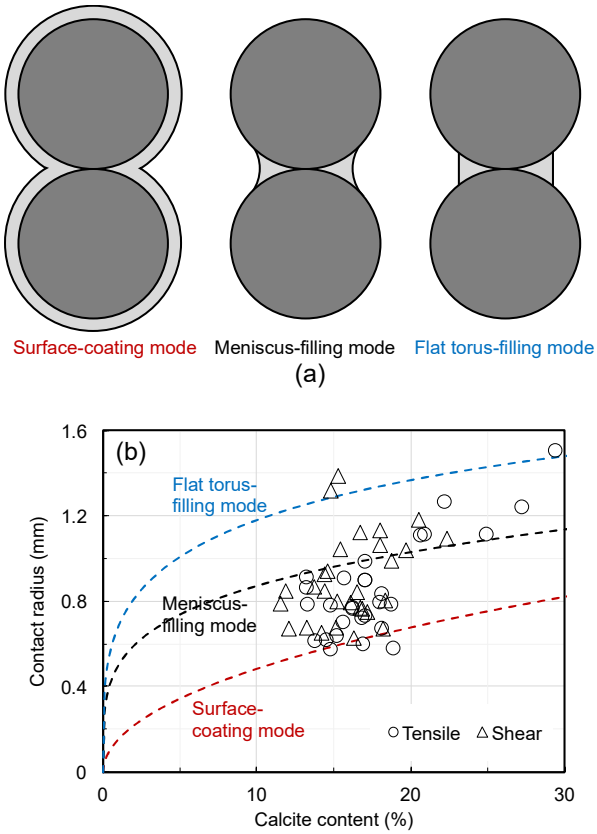

Figure 3. (a) Grain-scale precipitation patterns and (b) changes in contact radius with CaCO3 content at various precipitation pattern (modified from Ham et al., 2022).

4. Grain-scale Bonding Strength

4.1. Tensile and shear tests results

During the tensile and shear tests, the resistant force gradually increased while pulling, and it showed an abrupt reduction with a brittle failure. The maximum (or peak) force was used to estimate the maximum tensile and shear stresses applied until failure. Figure 4 shows the failures of bonded bead pairs by tensile loads at different CC levels. The maximum tensile and shear stress was calculated by dividing the peak force with the minimum cross-sectional area. The minimum cross-sectional area was almost proportional to CC.

Figure 5a shows the maximum tensile or shear stress measured for a CC level of the tested bead pair. The used

bead pairs appeared to have the CC range 10–30%, while majority is placed between 12–18%. The CC level of the bulk specimen was 17.5%. The tensile strength mostly ranged from 5 to 60 kPa, and the strength from 2 –30 kPa. The test results indicate that the MICP-induced bonds have the greater tensile strength than the shear strength though it differs with failure mode and cementation level.

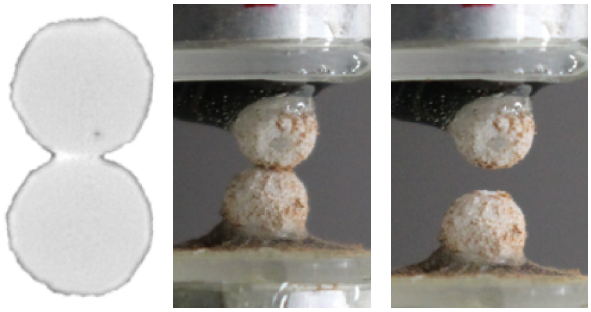

(a) Grain-coating pattern with CC = 14.5%

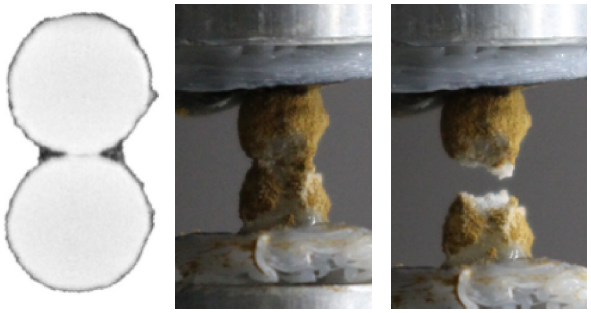

(b) Meniscus-filling pattern with CC = 24.9%

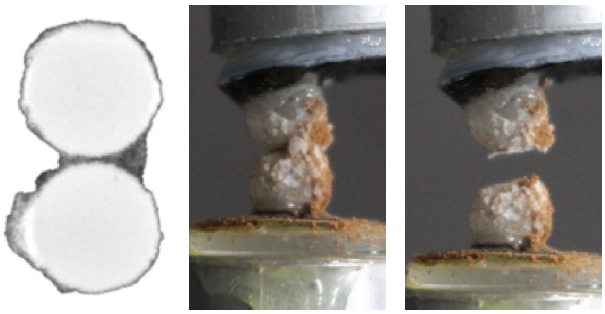

(c) Flat torus-filling pattern with CC = 27.2%

Figure 4. Images of MICP-treated two bead pairs at different level of cementations: (a) CC = 14.5%, (b) CC = 24.9%, and (c) CC = 27.2%. Note that the brown powder was sprayed on the bead pair prior to testing to visualize the failure surface.

4.2. Failure mechanisms

Failure surfaces on beads indicate three failure modes: debonding, internal, and mixed failure modes, as shown in Figure 5. Failure can occur at a precipitate-grain boundary as a debonding model, or an internal failure also can take place within the mass of precipitates. Or, a mixed mode of these debonding and internal failures can be observed. This was determined from the recorded digital images. As shown in Figure 5, for a given CC, the debonding failure required a higher force than the internal failure. This can be explained with the works required for internal failure and debonding failure, which is related to the surface energy between the calcite and glass bead. This is well consistent with the result reported by Montoya and Feng (2015) which have showed that debonding of the calcite from silica requires the larger work rather than the internal failure within calcite.

The occurrence of the failure modes is shown in Figure 6. The debonding and mixed failure modes were most frequently seen when CC < 20%. The tensile strength of 35 kPa and shear strength of 13 kPa were observed in average with the debonding failure mode. When CC > 20%, the internal failure mode became dominant and produced the lowest strength, which are ~8 kPa for tension and ~7 kPa for shear in average.

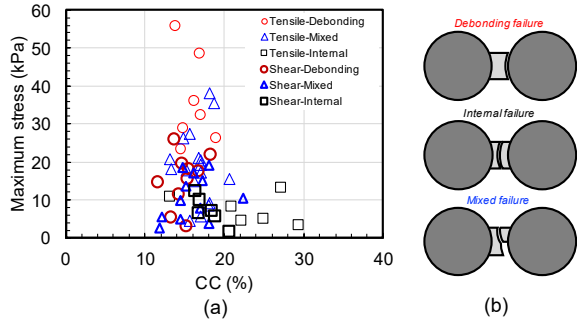

Figure 5. (a) Variations in maximum tensile and shear stresses with CC, and (b) grain-scale failure patterns (modified from Ham et al., 2022).

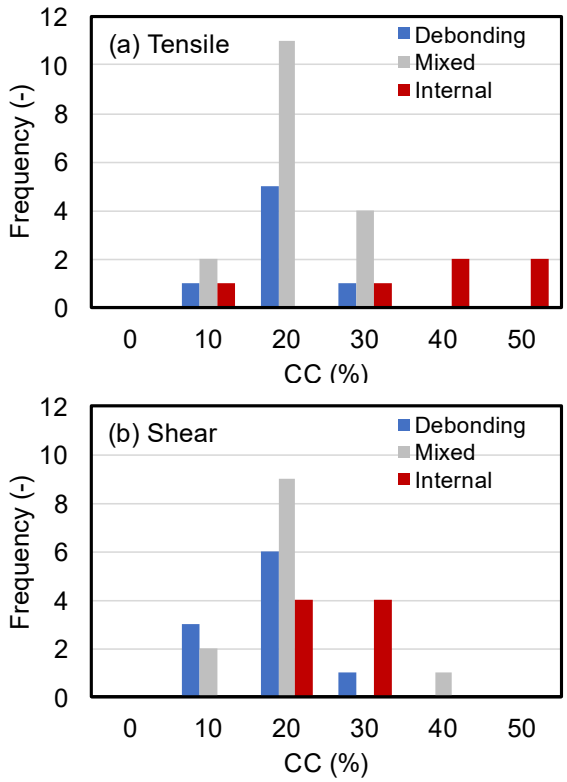

Figure 6. Distributions of failure modes: from (a) tensile tests and (b) shear tests (adopted from Ham et al., 2022).

5. Conclusions

This study explored the pore-scale precipitation patterns in MICP-treated sands and the grain-scale tensile and shear strengths of two beads cemented by MICP. The surface area, number of contacts, and flow-induced shear detachment as well as bacterial cell loci had a profound effect on the pore-scale precipitation. In fine sands, preferential precipitation was observed at grain contacts

and small pores, dominantly a contact-cementation pattern. By contrast, a surface-coating habit was mostly observed in coarse sands. Particularly, for large-sized grains, the precipitation pattern was found to evolve from the surface-coating mode to the flat-torus-filling mode with an increase in CC.

For the tested CC range from 10–30%, the MICP-induced bonds showed the greater tensile strength than the shear strength. The failure with MICP bonding occurred in three modes: debonding, internal, and mixed failure modes. The debonding and mixed failure modes most likely occurred when CC < 20%, in which the debonding failure showed the greatest strength, the tensile strength of 35 kPa and shear strength of 13 kPa. When CC > 20%, the internal failure mode became dominant, but the resulting strength was low as ~8 kPa for tension and ~7 kPa for shear in average. This is because the debonding failure needs to overcome a higher surface energy than the internal failure. The presented results advance insights into pore-scale and grain-scale behavior of MICP-treated sands.

Acknowledgements

This work was supported by "Ministry of the Interior and Safety" R&D program (20018265), and by the National Research Foundation of Korea (NRF) grant funded by the Korea government (MSIT) (NRF-2022R1A4A5031447).

References

Al Qabany, A., Soga, K. “Effect of chemical treatment used in MICP on engineering properties of cemented soils”, Géotechnique, 63(4), pp. 107–115, 2014.

Baek S. “Microbially Induced Calcite Precipitation (MICP): From Pore-scale Cementation Patterns to Their Effect on Hydraulic Conductivity and Suffusion Control”, Ph.D. Thesis, Korea Advanced Institute of Science and Technology (KAIST), Republic of Korea, 2022.

Baek S., Kwon, T.H., DeJong, J.T. "Reductions in hydraulic conductivity of sands caused by microbially induced calcium carbonate precipitation (MICP).", Journal of Geotechnical and Geoenvironmental Engineering, 2023. (in review)

Bick, P., Bastola, H., Suleiman, M.T., Gu, J., Diplas, P., Brown, D.G. and Zouari, N. "Minimizing wind erosion using microbial induced carbonate precipitation." In Geo-Congress 2019: Soil Improvement, pp. 223-230. Reston, VA: American Society of Civil Engineers, 2019.

Cheng L, Cord-Ruwisch R, Shahin MA. “Cementation of sand soil by microbially induced calcite precipitation at various degrees of saturation”, Canadian Geotechnical Journal, 50(1), pp. 81–90, 2013.

Choi, S. G., Chu, J., Brown, R.C., Wang, K., Wen, Z. “Sustainable biocement production via microbially induced calcium carbonate precipitation: use of limestone and acetic acid derived from pyrolysis of lignocellulosic biomass”, ACS Sustainable Chemistry & Engineering, 5(6), pp. 5183–5190, 2017.

Darby, K., Hernandez, G., Dejong, J., Boulanger, R., Gomez, M., and Wilson, D. “ Centrifuge Model Testing of Liquefaction Mitigation via Microbially Induced Calcite Precipitation”, Journal of Geotechnical and Geoenvironmental Engineering, 145(10), 2019.

DeJong, J.T., Fritzges, M. B., Nüsslein, K. “ Microbially induced cementation to control sand response to undrained shear”, Journal of Geotechnical and Geoenvironmental Engineering, 132(11), 1381–1392, 2006.

DeJong, J.T., Mortensen, B.M., Martinez, B.C., Nelson, D.C. “Bio-mediated soil improvement”, Ecological Engineering, 36(2), pp. 197–210, 2010.

DeJong, J.T., Gomez, M.G., San Pablo, A.C., Graddy, C.M.R., Nelson, D.C., Lee, M., Ziotopoulou, K., El Kortbawi, M., Montoya, B. and Kwon, T.H., 2022. "State of the Art: MICP soil improvement and its application to liquefaction hazard mitigation", Proceedings of the 20th ICSMGE-State of the Art and Invited Lectures, 2022.

Gao, K., Lin, H., Suleiman, M.T., Bick, P., Babuska, T., Li, X., Helm, J., Brown, D.G., Zouari, N. "Shear and Tensile Strength Measurements of CaCO 3 Cemented Bonds between Glass Beads Treated by Microbially Induced Carbonate Precipitation", Journal of Geotechnical and Geoenvironmental Engineering, 149(1), pp. 04022117, 2023.

Gomez, M.G., Martinez, B.C., DeJong, J.T., Hunt, C.E., deVlaming, L.A., Major, D.W. and Dworatzek, S.M., "Field-scale bio-cementation tests to improve sands." Proceedings of the Institution of Civil Engineers-Ground Improvement 168(3): 206-216, 2015.

Ham, S. M., Martinez, A., Han, G., Kwon, T. H. “Grain-scale tensile and shear strengths of glass beads cemented by MICP”, Journal of Geotechnical and Geoenvironmental Engineering, 148(9), pp. 04022068, 2022.

Harkes, M., Van Paassen, L., Booster, J., Whiffin, V., and van Loosdrecht, M. "Fixation and distribution of bacterial activity in sand to induce carbonate precipitation for ground reinforcement." Ecological Engineering 36(2): 112-117, 2010.

Lin, H., Suleiman, M. T., Brown, D. G., Kavazanjian Jr, E. “Mechanical behavior of sands treated by microbially induced carbonate precipitation”, Journal of Geotechnical and Geoenvironmental Engineering, 142(2), pp. 04015066, 2016.

Mahawish, A., Bouazza, A. and Gates, W.P., “Unconfined compressive strength and visualization of the microstructure of coarse sand subjected to different biocementation levels” Journal of Geotechnical and Geoenvironmental Engineering, 145(8), p.04019033, 2019.

Mitchell, A.C., Ferris, F.G. “The coprecipitation of Sr into calcite precipitates induced by bacterial ureolysis in artificial groundwater: temperature and kinetic dependence” Geochimica et Cosmochimica Acta, 69(17), pp. 4199–4210, 2005.

Montoya, B., Feng, K. “Deformation of microbial induced calcite bonded sands: a micro-scale investigation”, In: the sixth international symposium on deformation characteristics of geomaterials, Buenos Aires, 2015.

Nafisi, A., Safavizadeh, S.,Montoya, B. “Influence of Microbe and Enzyme-Induced Treatments on Cemented Sand Shear Response”, Journal of Geotechnical and Geoenvironmental Engineering, 145(9), 2019.

Seifan, M., Berenjian, A. “Microbially induced calcium carbonate precipitation: a widespread phenomenon in the biological world”, Applied Microbiology and Biotechnology, 103(12), pp. 4693–4708, 2019.

Sturm, A.P. “On the liquefaction potential of gravelly soils: Characterization, triggering and performance.” Ph.D. dissertation, Dept. Civil and Environmental Engineering, Univ. of California, Davis, U.S.A., 2019.

Pires-Sturm, A.P. and DeJong, J.T. “Influence of particle size and gradation on liquefaction potential and dynamic response.” Journal of Geotechnical and Geoenvironmental Engineering, 148(6): 04022045, 2022.

Terzis, D. and Laloui, L. “3-D micro-architecture and mechanical response of soil cemented via microbial-

induced calcite precipitation", Scientific Reports, 8(1), pp.1-11, 2018.

van Paassen, L. "Bio-mediated ground improvement: from laboratory experiment to pilot applications", In: Geo-Frontiers 2011: Advances in Geotechnical Engineering, 2011, pp. 4099-4108.

van Paassen, L.A., Ghose, R., van der Linden, T.J., van der Star, W.R. and van Loosdrecht, M.C. "Quantifying biomediated ground improvement by ureolysis: large-scale biogrout experiment", Journal of Geotechnical and Geoenvironmental Engineering, 136(12), pp.1721-1728, 2010.

Whiffin, V. S., Van Paassen, L. A.,Harkes, M. P. "Microbial carbonate precipitation as a soil improvement technique", Geomicrobiology Journal, 24(5), pp. 417–423, 2007.

Zhao, Q., Li, L., Li, C., Li, M., Amini, F., Zhang, H. "Factors affecting improvement of engineering properties of MICP-treated soil catalyzed by bacteria and urease", Journal of Materials in Civil Engineering, 26(12), pp. 04014094, 2014.